Journal of The Electrochemical Society, **146** (3) 862-868 (1999)
S0013-4651(98)08-006-9 CCC: $7.00

$LiAl_yCo_{1-y}O_2$ ($R\bar{3}m$) Intercalation Cathode for Rechargeable Lithium Batteries

Young-Il Jang,[a,*] Biying Huang,[a,] Haifeng Wang,[a] Donald R. Sadoway,[a,**] Gerbrand Ceder,[a,**] Yet-Ming Chiang,[a,**,z] Hui Liu,[b] and Hirokazu Tamura[b]**

[a]*Department of Materials Science and Engineering, Massachusetts Institute of Technology, Cambridge, Massachusetts 02139, USA*
[b]*Furukawa Electric Company, Limited, Yokohama Research Center, Yokohama 220, Japan*

$LiAl_yCo_{1-y}O_2$ solid solutions of α-$NaFeO_2$ structure type have been synthesized from homogeneous hydroxide precursors. X-ray powder diffraction and scanning transmission electron microscopy show that single-phase solid solutions are formed up to $y \approx 0.5$ at 800°C in air. Electrochemical tests using nonaqueous liquid electrolyte cells shows that the open-circuit voltage and working voltage increase with Al content as predicted by ab initio calculations [Ceder et al., *Nature*, **392**, 694 (1998)],[1] while capacity fade was significant during cycling at room temperature. However, both the absolute capacity and cycleability were improved at 55°C.

Manuscript submitted August 4, 1998; revised manuscript received September 15, 1998.

$LiCoO_2$ is currently in widespread use as a cathode material for rechargeable Li-ion batteries.[2] Due to its high cost, however, other materials such as $LiNiO_2$ and $LiMn_2O_4$ are being extensively studied as lower cost substitutes, as reviewed in Ref. 3. Efforts have also been made to synthesize solid solutions of $LiM_yCo_{1-y}O_2$ (M = transition metal) isostructural with $LiCoO_2$ in order to develop cathode materials with low cost, high energy density, excellent cycle life, and safety characteristics.[4-6] Recently, Ceder et al.[1] identified Al as a potentially attractive dopant that increases the intercalation voltage of $LiCoO_2$ while lowering density and cost. The present work reports in detail experimental synthesis, electrochemical characterization, and structural and chemical characterization of these materials.

Previously Al had received less attention as a solid solution constituent than transition metal elements because it was considered electrochemically inactive due to its fixed valence, leading to reduced specific capacity.[7-10] For instance, Ohzuku et al.[9,10] observed that doping with Al improves overcharge resistance in $LiAl_{0.25}Ni_{0.75}O_2$. Assuming that the amount of Li that can be deintercalated is limited by the transition metal fraction, they attributed the enhanced overcharge resistance to the formation of an insulator of $Li_{0.25}Al_{0.25}Ni_{0.75}O_2$ at the end of charging. On the other hand, Nazri et al. found that >95% Li deintercalation was possible during the first charge in $LiNi_{0.65}Al_{0.35}O_2$.[8] The recent theoretical discovery[1,11] that significant electron transfer to oxygen can occur by rehybridization of metal-oxygen atomic orbitals indicated that the conventional views of electron transfer occurring solely between transition metal ions should be revised, and that nontransition metals, including Al, could be considered "electrochemically active." A critical test of this theoretical result was the experimental confirmation that $LiAl_yCo_{1-y}O_2$ has an increased equilibrium voltage relative to $LiCoO_2$.[1] Here we examine the solid solubility of Al in $LiCoO_2$, the corresponding electrochemical properties, and the structure of the cathode oxide before and after electrochemical cycling.

Experimental

In a previous paper,[12] the synthesis of undoped $LiCoO_2$ by a method involving the decomposition and intercalation of hydroxides was reported. This method yields highly ordered "HT-$LiCoO_2$" by solid-state reaction at 300-400°C, with excellent electrochemical properties.[13] Here we extended this technique to $LiAl_yCo_{1-y}O_2$ solid solutions. $LiOH{\cdot}H_2O$ (Alfa Aesar, 98%), $Co(NO_3)_2{\cdot}6H_2O$ (Alfa Aesar, 99.5%), and $Al(NO_3)_3{\cdot}9H_2O$ (Alfa Aesar, 98%) were used as starting materials. Homegeneously mixed Al-Co hydroxides were coprecipitated by adding aqueous solutions of $Co(NO_3)_2$ and $Al(NO_3)_3$ mixed in the desired molar ratios, at an overall concentration of 0.2 M, to a stirred aqueous solution of LiOH. The LiOH solution was continuously monitored and titrated to keep the pH at 10.5. By using LiOH as the reactant, contamination of the product by impurities (e.g., other alkalis) is minimized. The nitrate solutions were prepared with Al/(Al+Co) ratios of 0, 0.25, 0.5, and 0.75. The precipitation conditions provide for nearly complete insolubility of aluminum and cobalt hydroxides.[14] The coprecipitated hydroxides were purified of nitrate species by repeated rinsing as described in Ref. 12. The precipitate was then dispersed in an aqueous solution of LiOH yielding a total Li:(Al+Co) ratio of 1.05:1. This suspension was atomized into liquid nitrogen, and the frozen droplets were freeze-dried (VirTis Consol 12LL, Gardiner, NY). Precursor powders were fired for 2 h at 300 to 800°C in air. The calcined powders were characterized by transmission electron microscopy (TEM) (JEOL 200CX), scanning transmission electron microscopy (STEM)/energy dispersive X-ray spectrometer (EDX) (VG HG603), and X-ray diffraction (XRD) using Cu Kα radiation (Rigaku RTP500RC).

For electrochemical evaluation, cathodes were prepared by mixing together the oxide powders, carbon black (Cabot), graphite (Timcal America), and poly(vinylidene fluoride) (PVDF) (Aldrich) in the weight ratio of 78:6:6:10. PVDF was predissolved in γ-butyrolactone (Aldrich) before mixing with the other components. After the γ-butyrolactone was evaporated at 150°C in air, the components were compacted at about 400 MPa to form pellets 10-25 mg in weight and 0.5 cm^2 in cross-sectional area. The pellets were then dried at 140°C under primary vacuum for 24 h and transferred into an argon-filled glove box. The electrochemical test cell consisted of two stainless steel electrodes with a Teflon holder. Lithium ribbon of 0.75 mm thickness (Aldrich) was used as the anode. The separator was a film of Celgard 2400™ (Celgard, Charlotte, NC), and the electrolyte consisted of a 1 M solution of $LiPF_6$ in ethylene carbonate (EC) and diethyl carbonate (DEC). The ratio of EC to DEC was 1:1 by volume. All cell handling was performed in an argon-filled glove box. Charge-discharge studies were performed with a MACCOR automated test equipment (series 4000).

We also tested powders of composition $y = 0.25$ using three-electrode electrochemical cells. In these cells, the working electrode was the $LiAlyCo_{1-y}O_2$ composite electrode, and counter electrode and reference electrode were Li. The reference electrode and working electrode were separated from the counter electrode by a PVDF membrane. The electrolyte was 1 M $LiClO_4$ in EC and dimethyl carbonate (DMC). The ratio of EC to DMC was 1:1 by volume.

Results and Discussion

Figure 1 shows the XRD pattern of $LiAl_{0.25}Co_{0.75}O_2$ samples for isochronal firings (2 h) in air at temperatures ranging from 300 to 800°C. Even after firing at 300°C, the sample shows the characteristic lines for the α-$NaFeO_2$ structure, although the peaks are broad,

* Electrochemical Society Student Member.
** Electrochemical Society Active Member.
z E-mail: ychiang@mit.edu

S0013-4651(98)08-006-9 CCC: $7.00 © The Electrochemical Society, Inc.

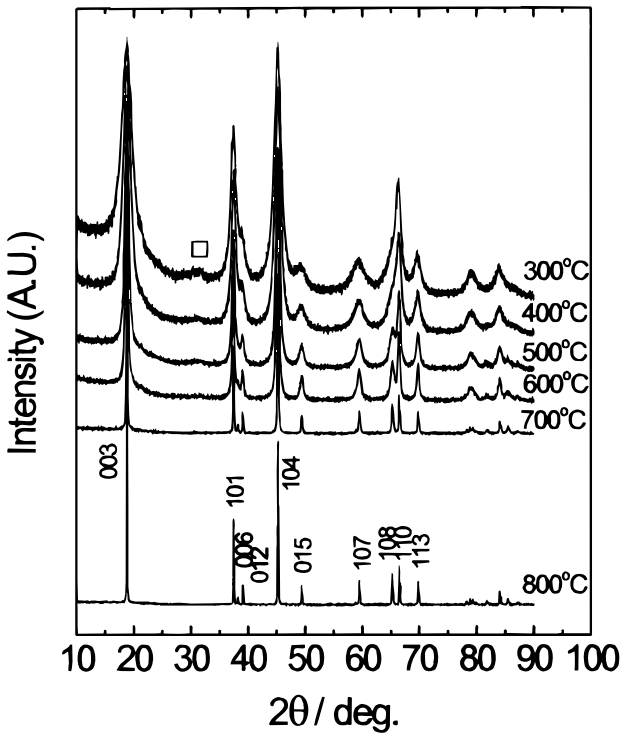

Figure 1. XRD patterns for $LiAl_{0.25}Co_{0.75}O_2$ obtained after firing for 2 h at various temperatures in air with *hkl* indicated for the 800°C-calcined sample (□: Li_2CO_3).

probably due to ultrafine crystallite size. There is a trace of Li_2CO_3 resulting from the exposure to CO_2 in the air. With increasing calcination temperature, the diffraction peaks sharpen, and after firing at

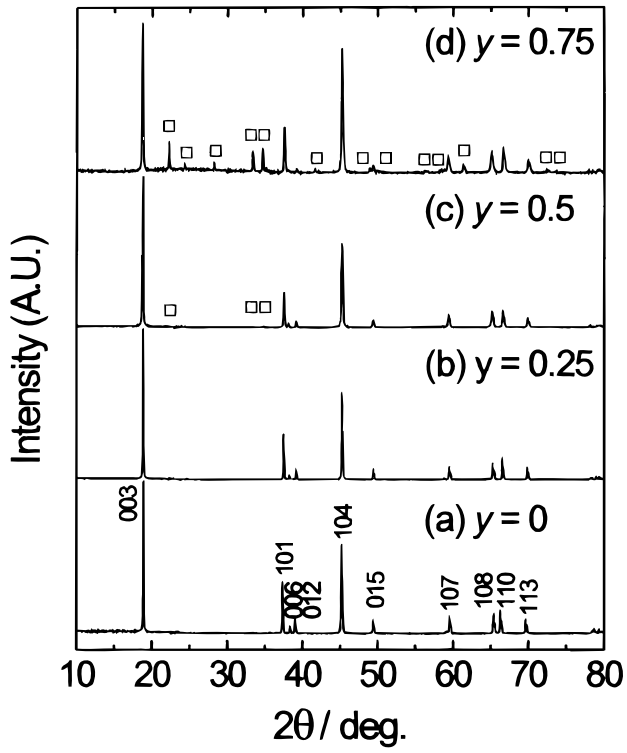

Figure 2. XRD patterns for $LiAl_yCo_{1-y}O_2$ obtained after firing for 2 h at 800°C in air for (a) $y = 0$, (b) 0.25, (c) 0.5, and (d) 0.75,with *hkl* indicated for $LiCoO_2$. (□: γ-$LiAlO_2$.)

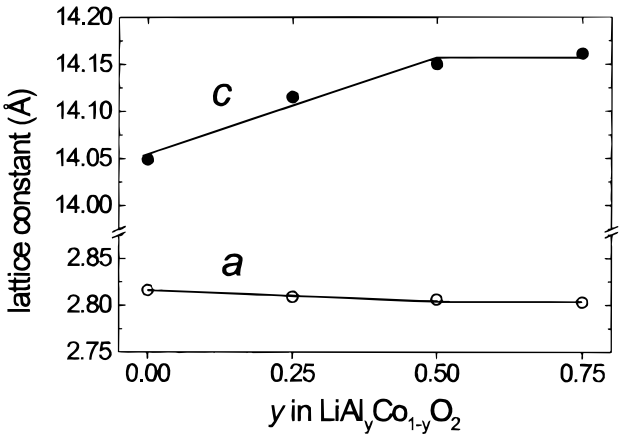

Figure 3. Lattice constants for $y = 0$, 0.25, 0.5, 0.75 in $LiAl_yCo_{1-y}O_2$ obtained after firing for 2 h at 800°C in air.

700-800°C for 2 h, we obtained a single-phase oxide, for which Miller indexes (*hkl*) are indexed for the hexagonal setting in Fig. 1. These coprecipitated precursors result in the "HT-$LiCoO_2$" structure upon firing at lower temperatures and shorter reaction time than is necessary in conventional solid-state reaction routes.[7]

XRD patterns for $LiAl_yCo_{1-y}O_2$ ($y = 0$, 0.25, 0.5, and 0.75) obtained after firing for 2 h at 800°C in air are shown in Fig. 2a-d, respectively. Samples with $y = 0$ and 0.25 are clearly single phase, and have the α-$NaFeO_2$ structure (space group $R\bar{3}m$). Peaks for γ-$LiAlO_2$ phase (space group $P4_12$) first appear with barely distinguishable intensity at $y = 0.5$, indicating that the solid solubility limit has just been exceeded. For $y = 0.75$, one can clearly see the γ-$LiAlO_2$ peaks in Fig. 2d. The appearance of γ-$LiAlO_2$ as the minor phase is consistent with the literature showing that γ-$LiAlO_2$ is the stable phase of undoped $LiAlO_2$ above 600°C.[15] With increasing y in $LiAl_yCo_{1-y}O_2$, the (006) and (108) peaks shift toward lower and the (110) peaks toward higher 2θ angles, resulting in a wider split of the (006)/(012) and (108)/(110) peaks compared with $LiCoO_2$. The lattice constants calculated by a least-square method from the XRD data are shown in Fig. 3 for samples corresponding to $y = 0$, 0.25, 0.5, and 0.75. Clearly, substitution of Al for Co results in shorter a and longer c. The evolution of lattice constants is continuous up to $y = 0.5$, and levels off between $y = 0.5$ and $y = 0.75$.

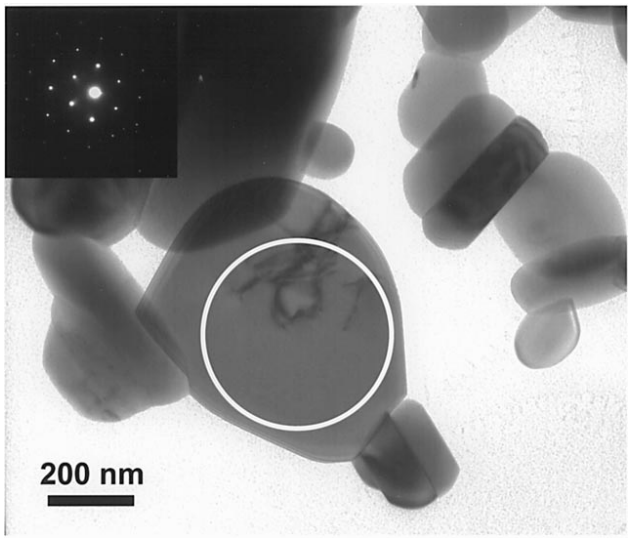

Figure 4. Bright-field TEM image and selected-area electron diffraction pattern obtained from the circled region of $LiAl_{0.25}Co_{0.75}O_2$ after firing for 2 h at 800°C in air.

S0013-4651(98)08-006-9 CCC: $7.00

Thus the powders are solid solutions until $y \approx 0.5$, after which two-phase mixtures are obtained.

The TEM bright-field image of $LiAl_{0.25}Co_{0.75}O_2$ powder fired for 2 h at 800°C in air is shown in Fig. 4. The particles have an equiaxed shape with diameters in the range of 0.1-0.5 μm. Shown in the inset is a selected-area diffraction pattern of a single particle taken with the beam along [0001], exhibiting the six-fold symmetry of the rhombohedral phase. Figure 5a shows a STEM bright-field image of $LiAl_{0.5}Co_{0.5}O_2$ powder fired for 2 h at 800°C in air, and Fig. 5b and c show the corresponding EDX elemental maps for Al and Co, respectively. Al and Co appear to be uniformly distributed throughout the particles. From the above results, we believe that Al can be ~50% substituted for Co in $LiCoO_2$ at 800°C in air. The solid solubility limit in our samples is higher than that reported by Nazri et al.[8] (~25% at 750°C). Still higher solubility may be obtained at a higher firing temperature.

The ab initio calculations[1,11] give the equilibrium potential of $LiAl_yCo_{1-y}O_2$ averaged over a certain Li concentration range. Complete intercalation curves have also been computed.[16] However, exact measurement of the equilibrium potential is difficult.[17] We used the observable open-circuit voltage (OCV) measured under a variety of conditions as a close approximation to the equilibrium potential. The OCV was measured by charging the cells at 0.05 mA/cm^2 to a specific Li content, then equilibrating for 15 h so that the rate of OCV change was less than 1 mV/h. Figure 6 shows the OCV thus measured as a function of composition for samples calcined for 2 h at 800°C in air. The data represent multiple cells for each composition. In calculating Li content from the charge capacity, we assumed 100% coulombic efficiency, that is

$$LiAl_yCo_{1-y}O_2 \rightarrow Li_{1-x}Al_yCo_{1-y}O_2 + xLi^+ + xe^- \qquad [1]$$

To examine the voltage characteristics of $LiAl_yCo_{1-y}O_2$ under working conditions, samples were charged to $Li_{0.6}Al_yCo_{1-y}O_2$, followed by discharge to $Li_{0.8}Al_yCo_{1-y}O_2$, at 0.4 mA/cm^2 (Fig. 7). Generally, the operating voltage V of a cell at a current I is

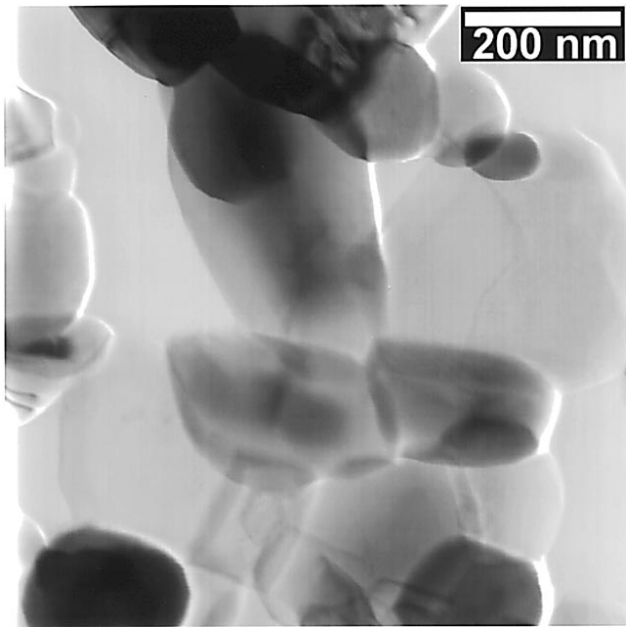

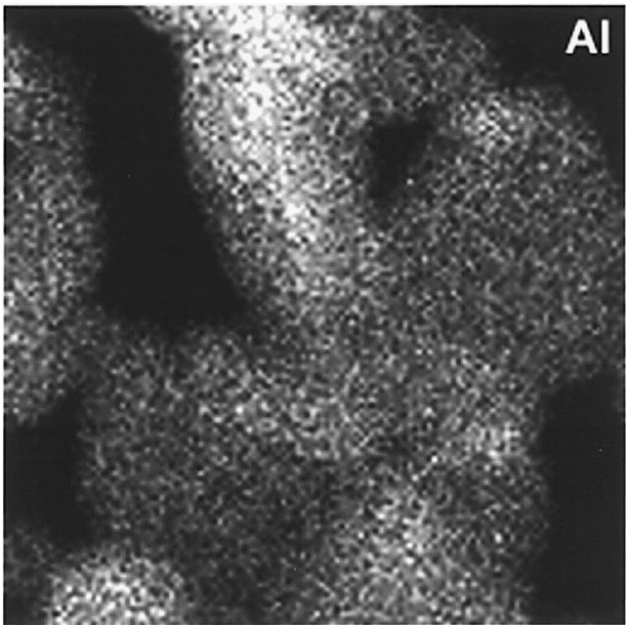

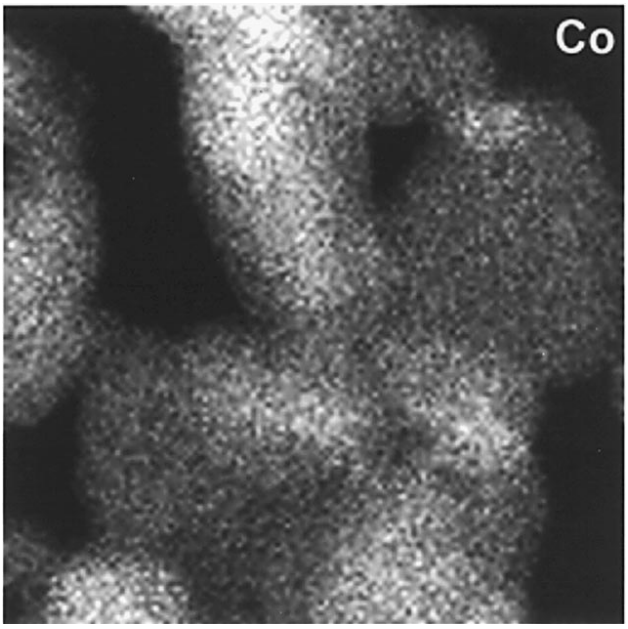

Figure 5. (a, top left) Bright-field STEM image and corresponding EDX elemental maps for (b, above) Al and (c, left) Co of $LiAl_{0.5}Co_{0.5}O_2$ after firing for 2 h at 800°C in air.

S0013-4651(98)08-006-9 CCC: $7.00

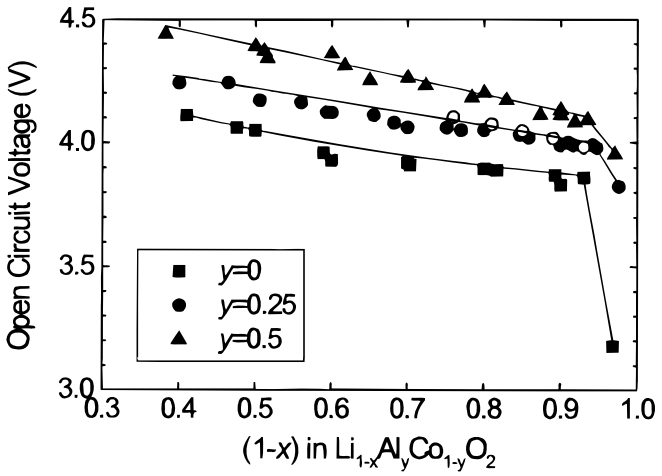

Figure 6. Open-circuit voltage (OCV) as a function of Li and Al contents in $Li_{1-x}Al_yCo_{1-y}O_2$ prepared by electrochemical oxidation of $LiAl_yCo_{1-y}O_2$ at 0.05 mA/cm^2. OCV was measured by charging nonaqueous cells at 0.05 mA/cm^2, then equilibrating for 15 h so that the rate of OCV change was less than 1 mV/h. The oxide samples were obtained by firing for 2 h at 800°C in air. (○: data obtained from the three-electrode cell.)

$$V = V_{oc} \pm IR \qquad [2]$$

where V_{oc} is the OCV and R is the internal resistance of the cell.[18] In Eq. 2, positive and negative signs correspond to charge and discharge conditions, respectively. It is apparent from Fig. 7 that the charge and discharge voltages of $LiAl_{0.25}Co_{0.75}O_2$ are both higher than those of $LiCoO_2$ by 0.15 to 0.20 V, showing that the voltage difference is not due to increased internal resistance or polarization.

Figure 8 shows OCV test results for the three-electrode cell of $y = 0.25$ powder, in which the cell was interrupted during charging and discharging (0.25 mA/cm^2) at 12.4 mAh/g intervals, and allowed to equilibrate for 10 h. This test shows that the OCV relaxes to the same value at each Li concentration during both charging and discharging (assuming 100% coulombic efficiency). Clearly the OCV is very close to the equilibrium value. The OCV as a function of Li content measured in this manner is also plotted in Fig. 6 and agrees well with the two-electrode cell tests. We conclude that Al doping increases the open-circuit voltage and working voltage of $LiCoO_2$ as predicted by the ab initio calculations.[1,11]

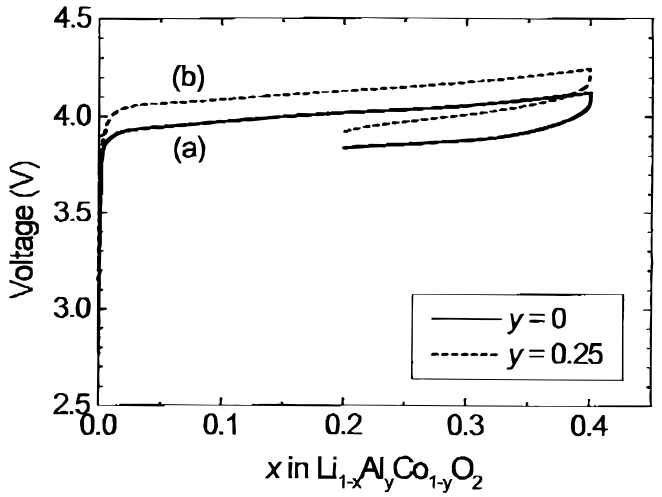

Figure 7. Voltage curves of $Li_{1-x}Al_yCo_{1-y}O_2$ in charging up to $x = 0.4$, followed by discharging to $x = 0.2$ at 0.4 mA/cm^2 for (a) $y = 0$ and (b) 0.25. The oxide samples were obtained by firing for 2 h at 800°C in air.

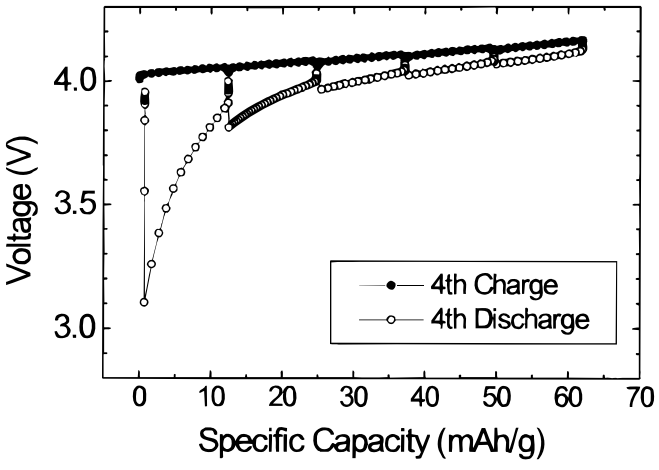

Figure 8. OCV test results for a cell corresponding to $y = 0.25$ that was interrupted during the 4th charging and discharging at 0.25 mA/cm^2 at every 12.4 mAh/g and allowed to equilibrate for 10 h. The oxide samples were obtained by firing for 2 h at 800°C in air.

XRD studies were carried out on cathode pellets in order to follow the change in structure of $Li_{1-x}Al_yCo_{1-y}O_2$ during charging. Figures 9 and 10 show the evolution of the XRD patterns of $Li_{1-x}Al_{0.25}Co_{0.75}O_2$ and $Li_{1-x}Al_{0.5}Co_{0.5}O_2$, respectively, as a function of x. The powders were fired at 800°C for 2 h in air. Compared with Fig. 3, the relative intensity of the (003) diffraction lines for the same powder prepared as a composite is stronger, which we attribute to some particle orientation introduced during mixing and pressing of the cathode mixtures.[17] Diffraction lines from carbon and PVDF are also detectable in the cathode mixtures. The (003) and (006)

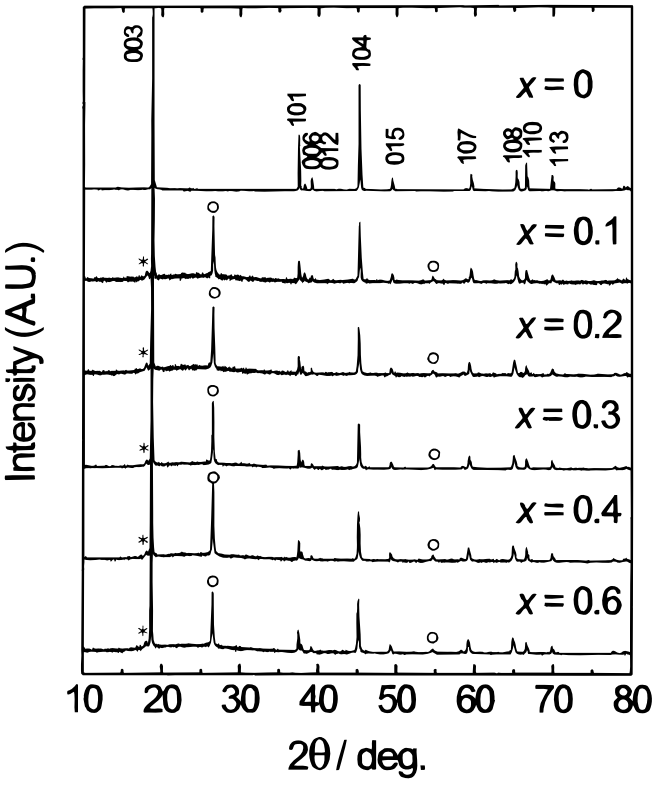

Figure 9. XRD patterns of $Li_{1-x}Al_{0.25}Co_{0.75}O_2$, with *hkl* indicated, prepared by the electrochemical oxidation of $LiAl_{0.25}Co_{0.75}O_2$ at 0.05 mA/cm^2. The oxide samples were obtained by firing for 2 h at 800°C in air. [(○: graphite, (*): PVDF.]

S0013-4651(98)08-006-9 CCC: $7.00

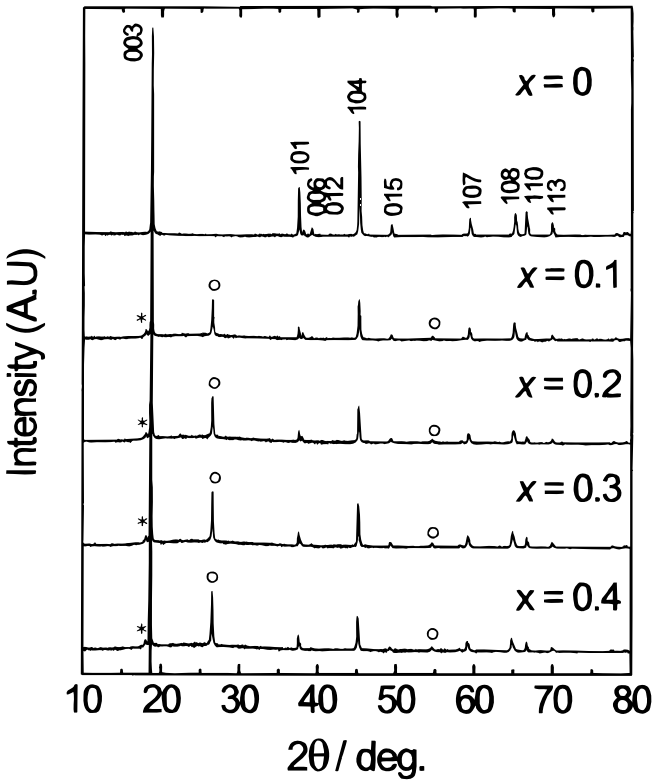

Figure 10. XRD patterns of $Li_{1-x}Al_{0.5}Co_{0.5}O_2$, with *hkl* indicated, prepared by the electrochemical oxidation of $LiAl_{0.5}Co_{0.5}O_2$ at 0.05 mA/cm^2. The oxide samples were obtained by firing for 2 h at 800°C in air. [(○): graphite, (*): PVDF.]

lines for the oxide shift toward lower 2θ diffraction angles during charging. Simultaneously, the (110) lines shift toward higher diffraction angles. However, neither line broadening nor appearance or disappearance of diffraction lines was observed. Lattice constants as a function of composition during first charging, determined from the XRD data, are shown in Fig. 11. General trends, such as the shrinkage of *a* and the expansion of *c* as *x* increases, are the same as previously reported for $Li_{1-x}CoO_2$,[19,20] although the variation in lattice constants of $Li_{1-x}Al_yCo_{1-y}O_2$ during charging (~1% and ~ −0.1% in *c* and *a*, respectively, up to $Li_{0.4}Al_yCo_{1-y}O_2$) is almost one-half

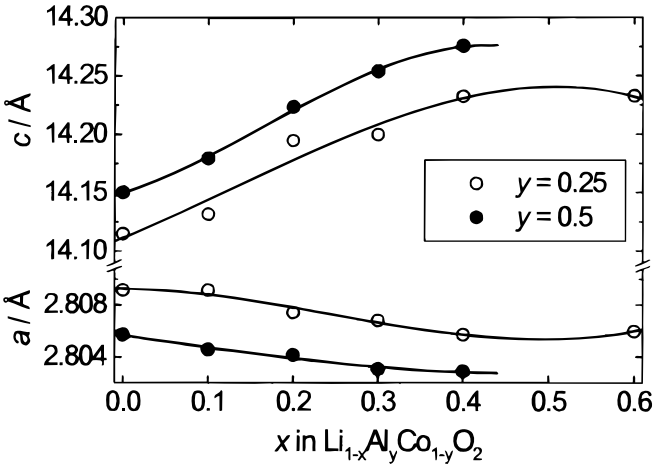

Figure 11. Change in lattice parameters, *a* and *c* in hexagonal setting, for $Li_{1-x}Al_{0.25}Co_{0.75}O_2$ and $Li_{1-x}Al_{0.5}Co_{0.5}O_2$ prepared by the electrochemical oxidation at 0.05 mA/cm^2. The oxide samples were obtained by firing for 2 h at 800°C in air.

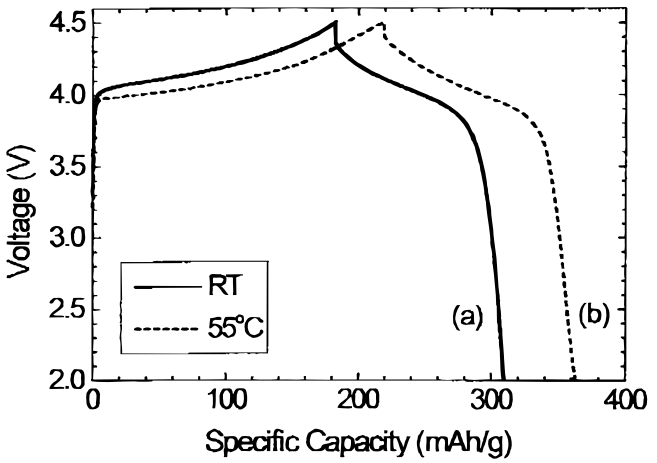

Figure 12. First charge-discharge curve for $LiAl_{0.25}Co_{0.75}O_2$, tested against a Li metal anode at 0.4 mA/cm^2 between 2.0 and 4.5 V at (a) room temperature and (b) 55°C. The oxide samples were obtained by firing for 2 h at 800°C in air.

that of pure $Li_{1-x}CoO_2$ (~2% and ~ −0.2% in *c* and *a*, respectively, up to $Li_{0.4}CoO_2$).[19] It is interesting to note that $y = 0.25$ and $y = 0.5$ show similar variation in lattice parameters upon delithiation, although the absolute values of *a* and *c* differ, suggesting that the lattice stabilization imparted from Al addition is essentially complete at $y = 0.25$.

$LiAl_{0.25}Co_{0.75}O_2$ electrodes were cycled at room temperature and 55°C in the two-electrode cells. Figure 12a and b show the first charge-discharge curves at room temperature and 55°C, respectively, between 2.0 and 4.5 V at 0.4 mA/cm^2. During the first charge, 182 mAh/g was extracted at room temperature, and 219 mAh/g at 55°C, corresponding to 61 and 73% of the theoretical capacity, respectively, assuming that Li can be removed completely from $LiAl_{0.25}Co_{0.75}O_2$ based on the metal-oxygen rehybridization theory.[1,11] The first-discharge capacities were 127 mAh/g (energy density 488 Wh/kg) and 144 mAh/g (554 Wh/kg) at room temperature and 55°C, respectively. Rapid capacity fade was observed upon cycling at room temperature as shown in Fig. 13. After nine cycles, the discharge capacity decreased to 51% of the initial value. However, the cell cycled at 55°C retains 72% of the initial discharge capacity, 104 mAh/g, after nine cycles.

We conducted XRD and TEM/STEM analysis of the cycled cathodes to observe structural and compositional damages due to elec-

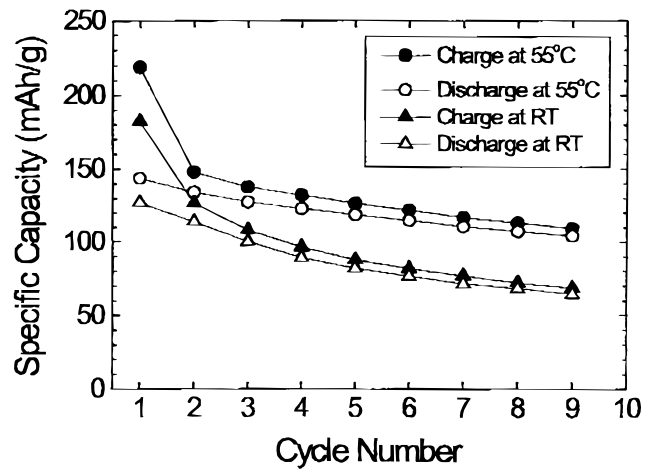

Figure 13. Specific capacity vs. cycle number for $LiAl_{0.25}Co_{0.75}O_2$, tested against a Li metal anode at 0.4 mA/cm^2 between 2.0 and 4.5 V at room temperature and 55°C. The oxide samples were obtained by firing for 2 h at 800°C in air.

S0013-4651(98)08-006-9 CCC: $7.00

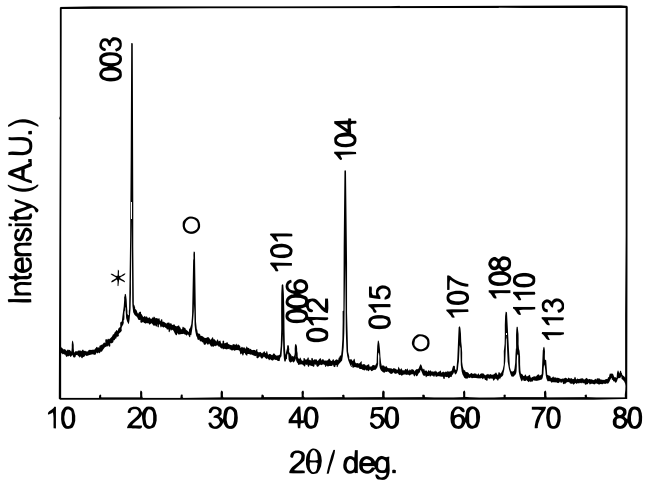

Figure 14. XRD pattern of $LiAl_{0.25}Co_{0.75}O_2$ electrode cycled 20 times against a Li metal anode at 0.4 mA/cm^2 between 2.0 and 4.4 V at room temperature. The oxide samples were obtained by firing for 2 h at 800°C in air. [(○): graphite, (*): PVDF.]

trochemical cycling. Figure 14 shows the XRD pattern of a $LiAl_{0.25}Co_{0.75}O_2$ cathode pellet after 20 cycles at room temperature between 2.5 and 4.4 V at a current density of 0.4 mA/cm^2. Comparing with Fig. 2b, one can see that the α-$NaFeO_2$ structure is retained. Figure 15 shows a TEM image and a selected-area diffraction pattern of oxide particles from the same pellet. Compared to the particles before electrochemical cycling (Fig. 4), the cycled particles have severe strain and high dislocation densities, indicated by diffraction contrast features within the particles. This damage is similar to that seen in a separate study of cycled $LiCoO_2$.[21] However, elemental maps for Al and Co in Fig. 16 show that a uniform solid solution is retained after cycling. Cycling of undoped $LiCoO_2$ between 2.5 and 4.3 V also causes a partial transformation to spinel disorder, detectable in selected-area electron diffraction of individual particles as the appearance of new {220} reflections.[21] In the cycled $LiAl_{0.25}Co_{0.75}O_2$, we rarely observed this disorder even though the charging voltage limit was higher (4.4 V) and the initial discharge capacity on a Li concentration basis equal to that in the $LiCoO_2$. This

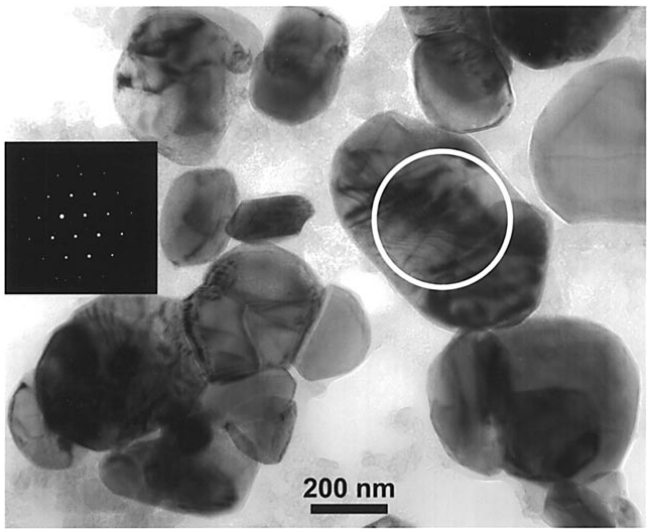

Figure 15. Bright field TEM image and selected-area electron diffraction pattern obtained from the circled region of $LiAl_{0.25}Co_{0.75}O_2$ electrode after cycling 20 times against a Li metal anode at 0.4 mA/cm^2 between 2.0 and 4.4 V at room temperature. The oxide samples were obtained by firing for 2 h at 800°C in air.

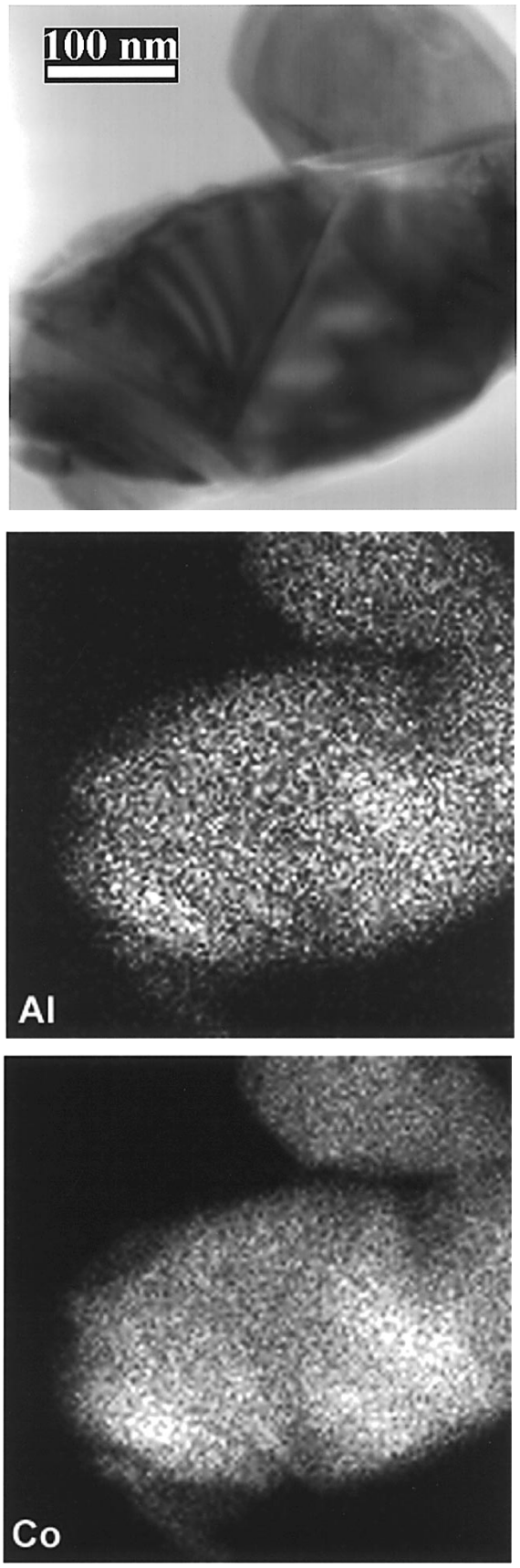

Figure 16. (a, top) Bright-field STEM image and corresponding EDX elemental maps for (b, middle) Al and (c, bottom) Co of $LiAl_{0.25}Co_{0.75}O_2$ electrode cycled 20 times against a Li metal anode at 0.4 mA/cm^2 between 2.0 and 4.4 V at room temperature. The oxide samples were obtained by firing for 2 h at 800°C in air.

S0013-4651(98)08-006-9 CCC: $7.00

suggests that Al may stabilize $LiCoO_2$ against the transformation to spinel during electrochemical cycling. The analyses conducted to date show that $LiAl_{0.25}Co_{0.75}O_2$ is stable in terms of its composition and structure during cycling. The cause of the capacity fade apparently lies elsewhere, and requires further study to understand.

Conclusions

$LiAl_yCo_{1-y}O_2$ solid solutions have been synthesized in the α-$NaFeO_2$ structure type using homogeneous hydroxide precursors prepared by a coprecipitation method. At 800°C, the solid-solution limit for Al was determined to be $y \approx 0.5$. The open-circuit voltage increases systematically with Al content in solid solution, verifying ab initio predictions.[1,11] The *c*/*a* ratio increases with Al concentration while the cell volume remains approximately unchanged. There exists a larger van der Waals gap in the Al-doped solid solutions compared to $LiCoO_2$ and a smaller variation in crystal dimension with Li concentration, suggesting that higher Li diffusivity and lower cycling-induced lattice strain are possible in $Li_{1-x}Al_yCo_{1-y}O_2$. In the present compositions, higher capacity and lower capacity fade were also observed at 55°C than at room temperature.

Acknowledgments

Helpful discussions with M. K. Aydinol, A. Van der Ven, and A. M. Mayes are gratefully acknowledged. This work was supported by the INEEL University Research Consortium and by Furukawa Electric Company, Limited. The INEEL is managed by Lockheed Martin Idaho Technology Company for the U.S. Department of Energy, Idaho Operations Offices, under contract no. DE-AC07-94ID13223. Instrumentation in the Shared Experimental Facilities at MIT, supported by NSF Grant No. 9400334-DMR, was also used. Y.I.J. also acknowledges a fellowship from the Ministry of Education, Korea.

Massachusetts Institute of Technology assisted in meeting the publication costs of this article.

References

1. G. Ceder, Y.-M. Chiang, D. R. Sadoway, M. K. Aydinol, Y.-I. Jang, and B. Huang, *Nature*, **392,** 694 (1998).
2. K. Ozawa, *Solid State Ionics*, **69,** 212 (1994).
3. R. Koksbang, J. Barker, H. Shi, and M. Y. Saïdi, *Solid State Ionics*, **84,** 1 (1996).
4. C. D. W. Jones, E. Rossen, and J. R. Dahn, *Solid State Ionics*, **68**, 65 (1994).
5. A. Ueda and T. Ohzuku, *J. Electrochem. Soc.*, **141,** 2010 (1994).
6. R. Stoyanova, E. Zhecheva, and L. Zarkova, *Solid State Ionics*, **73,** 233 (1994).
7. Q. Zhong and U. von Sacken, *J. Power Sources*, **54,** 221 (1995).
8. G. A. Nazri, A. Rougier, and K. F. Kia, *Mater. Res. Soc. Sym. Proc.*, **453,** 635 (1997).
9. T. Ohzuku, A. Ueda, and M. Kouguchi, *J. Electrochem. Soc.*, **142,** 4033 (1995).
10. T. Ohzuku, T. Yanagawa, M. Kouguchi, and A. Ueda, *J. Power Sources*, **68,** 131 (1997).
11. M. K. Aydinol, A. F. Kohan, G. Ceder, K. Cho, and J. Joannopoulos, *Phys. Rev. B*, **56,** 1354 (1997).
12. Y.-M. Chiang Y.-I. Jang, H. Wang, B. Huang, D. R. Sadoway, and P. Ye, *J. Electrochem. Soc.*, **145,** 887 (1998).
13. B. Huang, Y.-I. Jang, Y.-M. Chiang, and D. R. Sadoway, *J. Appl. Electrochem.*, **28**, 1365 (1998).
14. C. F. Baes, Jr. and R. E. Mesmer, *The Hydrolysis of Cations*, Krieger, Malabar, FL (1986).
15. H. A. Lehmann and H. Hesselbarth, *Z. Anorg. Allg. Chem.*, **313,** 117 (1961).
16. S. Buta, A. Van der Ven, M. K. Aydinol, and G. Ceder, Abstract 115, The Electrochemical Society Meeting Abstracts, Boston, Nov (1998), To be published.
17. A. Ueda and T. Ohzuku, *J. Electrochem, Soc.*, **141,** 2010 (1994).
18. J. B. Goodenough, *Solid State Ionics*, **69,** 184 (1994).
19. J. N. Reimers and J. R. Dahn, *J. Electrochem. Soc.*, **139,** 2091 (1992).
20. T. Ohzuku and A. Ueda, *J. Electrochem. Soc.*, **141,** 2972 (1994).
21. H. Wang, Y.-I. Jang, B. Huang, D. R. Sadoway, and Y.-M. Chiang, *J. Electrochem. Soc.*, **146,** 473 (1999).